

Electron correlation in the $4d$ hole state of Ba studied by Auger and photoelectron spectroscopy

A. Mäntykenttä, H. Aksela, and S. Aksela

Department of Physics, University of Oulu, SF-90570 Oulu, Finland

J. Tulkki and T. Åberg

Laboratory of Physics, Helsinki University of Technology, SF-02150 Espoo, Finland

(Received 29 October 1992)

Electron correlation in the $4d$ hole state of Ba has been studied by comparing the experimental $4d^{-1} \rightarrow 6s^{-2}$ Auger electron and $4d$ photoelectron spectrum with results based on the Bethe-Born approximation and relativistic multiconfiguration Dirac-Fock calculations. The $4d$ -hole-state correlation is found to result in a reversal of the $4d_{5/2}:4d_{3/2}$ branching ratio in going from the photoelectron spectrum to the Auger spectrum in accordance with experimental results.

PACS number(s): 32.80.Hd, 32.80.Fb

I. INTRODUCTION

Recent synchrotron-radiation studies [1, 2] of photoabsorption of outer shells in atomic Ba with the configuration $[\text{Kr}]4d^{10}5s^25p^66s^2$ demonstrate that there are still many open questions regarding the many-electron excitation dynamics of the electrons outside the Kr core. Two major factors which contribute to the complexity of the spectra are (i) collapse of the empty $5d$ and $4f$ subshell wave functions and (ii) change of the correlated motion of the $6s$ electrons upon excitation and ionization [3]. Related phenomena with appropriate modifications of the principal and orbital quantum numbers occur in other alkaline-earth-metal atoms as well [3, 4].

Figure 1 shows measured $4d^{-1} \rightarrow 5p^{-2}$ Auger spectra of Xe, Cs, and Ba in comparison with single-configuration average-level Dirac-Fock intermediate-coupling calculations. The independent-particle approach predicts only slight changes in the intensity distribution as Z increases from 54 to 56 in contrast to the experimental results. The Ba $4d^{-1} \rightarrow 5p^{-2}$ spectrum, which does not resemble the Xe and Cs spectra at all, serves here as an illustration of conspicuous many-electron correlation effects in alkaline-earth-metal spectra.

Mehlhorn, Breuckmann, and Hausmann [5] have pointed out that a full interpretation of the $4d$ Auger electron emission spectrum of Ba requires simultaneous considerations of initial-state (ISCI), initial-ionic-state (IISCI), and final-ionic-state configuration interaction (FISCI). They attribute a part of the complexity of the spectrum to the collapse of the $5d$ orbital upon removal of the $4d$ electron. For the $3d^{-1} \rightarrow 4d^{-2}$ Auger spectrum it has been found that $3d^{-1}(6s^2 + 6s5d + 5d^2)$ IISCI in combination with $4d^{-2}(6s^2 + 6s5d + 5d^2)$ FISCI leads to a reasonable interpretation of the line structure [6]. The inclusion of the $4s^2 + 3d4s + 3d^2$ manifold in both IISCI and FISCI also improves the agreement between multiconfiguration Dirac-Fock (MCDF) calculations and experiments in the case of some Ca $2p$ Auger transitions [4].

In this work we shall investigate within the MCDF approach how the mixing between the $6s^2$, $6s5d$, $5d^2$, $6p^2$, and $4f^2$ configurations influences the $4d^{-1} \rightarrow 6s^{-2}$ Auger transitions in Ba. All these transitions correspond

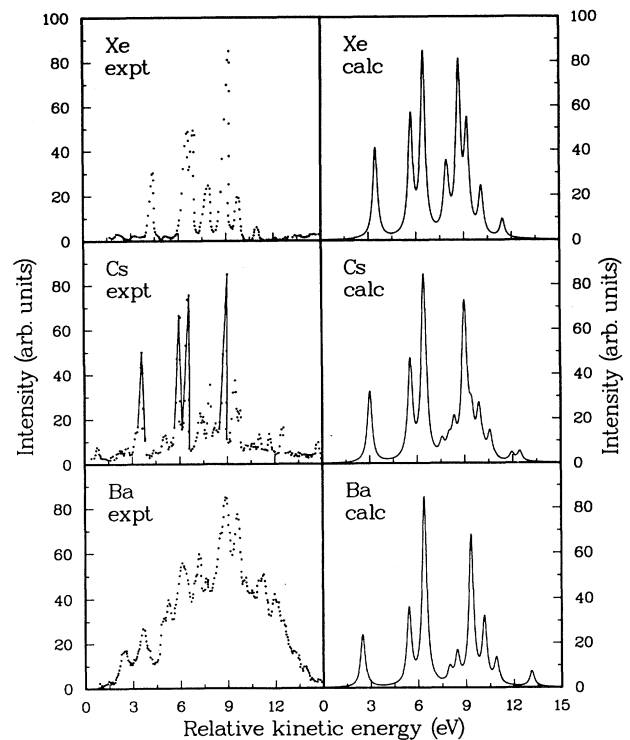


FIG. 1. Experimental $4d^{-1} \rightarrow 5p^{-2}$ Auger electron spectra in comparison with calculated spectra for Xe, Cs, and Ba. The kinetic energy of the Auger electron is given on a relative scale in which the experimental and calculated positions of the most intense peak coincide. The absolute experimental energy of this peak is 34.3 eV for Xe, 38.5 eV for Cs, and 42.7 eV for Ba. In the calculated spectra the most intense peak is at 33.0 eV for Xe, 37.0 eV for Cs, and 41.3 eV for Ba.

to the final $[\text{Kr}]4d^{10}5s^25p^6$, $J = 0$ ionic state which does not involve appreciable $6s^2$ mixing. Any anomalies in the spectrum are thus expected to be a consequence of IISCI in which the $5d$ and $4f$ wave function collapse plays a fundamental role. The same configuration interaction (CI) should also affect the final states in the $4d$ photoelectron spectrum. We shall therefore investigate both spectra which without CI should only exhibit two peaks, separated by $4d$ spin-orbit interaction and having an intensity ratio of 3 to 2. We shall demonstrate the breakdown of the independent-particle approach and thereby provide an interpretation of the reversal of the $4d_{5/2}:4d_{3/2}$ branching ratio in going from the photoelectron to the Auger spectrum. Since the initial ionic $4d$ hole states of the Auger transitions are residual final ionic states in photoionization we shall use the acronym IMISCI (intermediate-ionic-state configuration interaction) to denote the correlation in these states.

II. EXPERIMENT

The $4d$ Auger spectra have been measured with a cylindrical mirror-type electron spectrometer at the University of Oulu. The Ba atoms were ionized with 3-keV electrons, and electrons emitted in an angle of 54.7° with respect to the primary beam were observed. The energy scale was calibrated against accurately known Kr Auger lines. Temperature and vapor pressure were varied and different oven materials (stainless steel, graphite) were used. No changes in the peak intensities were observed, indicating that the $4d$ spectra are free from chemical effects. Our $4d^{-1} \rightarrow 5p^{-2}$, $5s^{-1}6s^{-1}$, $5p^{-1}6s^{-1}$, and $6s^{-2}$ spectra, shown in Fig. 2, are in very good agreement with the 2 keV-electron excited spectra of Mehlhorn, Breuckmann, and Hausmann [5]. The overall shape of our experimental spectra is also similar to the shape found by Bizau *et al.* [2] in their synchrotron-radiation ($h\nu = 130$ eV) experiment and by Richter *et al.* [1] in their measurement with 110.4-eV photons. This indicates that structural details in these spectra are independent of primary excitation.

The $4d^{-1} \rightarrow 6s^{-2}$ spectrum which exhibits four peaks is shown in detail in Fig. 3(a). The doublet 1,2 is due to

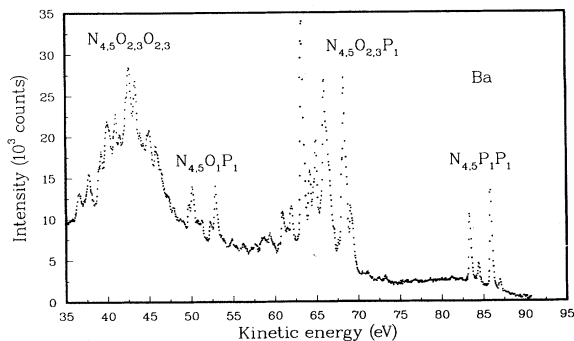


FIG. 2. The Ba $4d$ Auger spectrum excited by 3-keV electron impact.

$4d_{5/2}$ Auger transitions and the doublet 3,4 to $4d_{3/2}$ transitions. The energy difference between the doublet components 1 and 3 as well as 2 and 4 is equal to $4d$ spin-orbit splitting 2.6 eV. The ratio of the integrated intensities of the $4d_{5/2}$ and $4d_{3/2}$ peaks [(peak 1 plus peak 2):(peak 3 plus peak 4)] is 0.8 ± 0.2 , which clearly deviates from the statistical ratio 1.5. In contrast, the branching ratio of the $4d_{5/2}$ and $4d_{3/2}$ photoelectron peaks has been found to be closer to the statistical ratio well above the threshold of ionization [7]. Between $h\nu = 120$ and 150 eV it has been found to be 1.2 ± 0.2 [7], in good agreement with the relativistic random-phase approximation [8]. We have checked this finding by remeasuring the $4d$ photoelectron spectrum using synchrotron radiation at the Photon Factory in Tsukuba, Japan [9]. Our result for

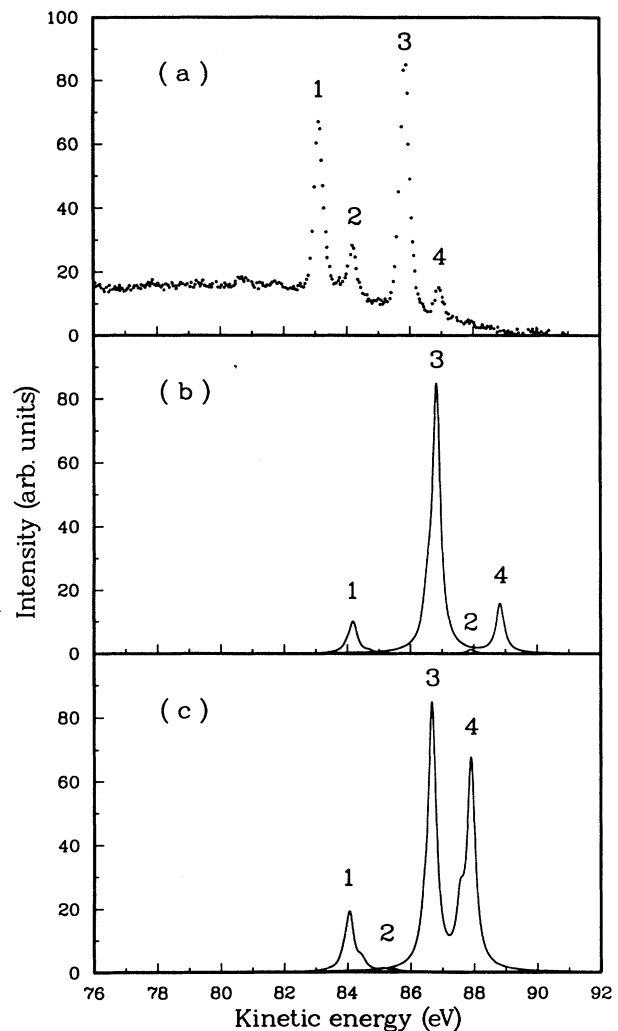


FIG. 3. The Ba $4d_{5/2,3/2} \rightarrow 6s^{-2}$ Auger electron spectrum: (a) experiment, (b) truncated-set calculation, and (c) calculation, based on set (11). Peak 3 has been normalized to the same height in all spectra. The peaks 1 and 2 are associated with the $4d_{5/2}$ hole, and peaks 3 and 4 with the $4d_{3/2}$ hole.

the ratio of the integrated intensities (peak 1:peak 3) is 1.2 ± 0.2 . The spectrum shown in Fig. 4(a) was obtained at $h\nu = 135$ eV and at an angle $\theta_p = 54.7^\circ$ with respect to the electric-field vector. The overall agreement with earlier experiments [1, 2, 7] is excellent. Photon peaks 1 and 2 are associated with $4d_{5/2}$ and peaks 3 and 4 with $4d_{3/2}$ photoionization. Additional satellites 5–7 appear at the low kinetic-energy side. Their pattern is quite complicated but 5 and 6 can be mainly attributed to $4d_{5/2}$, whereas 7 seems to belong to $4d_{3/2}$ [9]. The similarity between the 4d Auger spectra excited by 130-eV photons and 3-keV electrons was also checked and was found to be excellent. The anomalous branching ratio of the Auger peaks thus is independent of the primary excitation. It is considerably lower than the $4d_{5/2}:4d_{3/2}$ ratio of the corresponding photopeaks, recorded at the same photon energy.

III. THEORY

The relative number of emitted Auger electrons per unit time has been calculated using a two-step model in which the primary 4d ionization of the Ba atom is assumed to take place independently of the radiationless and radiative decay of the 4d hole states. We represent a hole-state wave function by the expansion

$$\Psi_\beta(J_\beta M_\beta) = \sum_\nu c_{\beta\nu} \Phi_\nu(J_\beta M_\beta), \quad (1)$$

where the functions $\Phi_\nu(J_\beta M_\beta)$ are configuration-state functions (CSF's), each of which corresponds to a pure jj -coupled state of same parity. In the MCDF method the orbitals used to construct the atomic-state functions (ASF's) $\Psi_\beta(J_\beta M_\beta)$ can be determined by several procedures. In this work we have used the average-level (AL) scheme which is based on a variational calculation involving the average energy of all CSF's in Eq. (1). Similar expressions can be written for the ground-state wave function $\Psi_i(J_i M_i)$ and for the final-ionic-state wave functions $\Psi_f(J_f M_f)$. For Ba $J_i = M_i = 0$, and for the particular final ionic state of Ba^{2+} considered in this work we also have $J_f = M_f = 0$. The following development is general, however, except for Eq. (6).

The relative number of emitted Auger electrons in ionization of randomly oriented atoms by high-energy electron impact is given by

$$n_{f\beta}(J_f J_\beta; \theta) = \sum_{M_f, M_\beta} T_{f\beta}(J_f M_f, J_\beta M_\beta; \theta) \times \frac{Q_\beta(J_\beta M_\beta) N_i}{P_\beta(J_\beta)}, \quad (2)$$

where θ is the angle of Auger electron emission with respect to the direction of the primary beam, consisting of N_i electrons per unit time and area and where $P_\beta(J_\beta)$ is

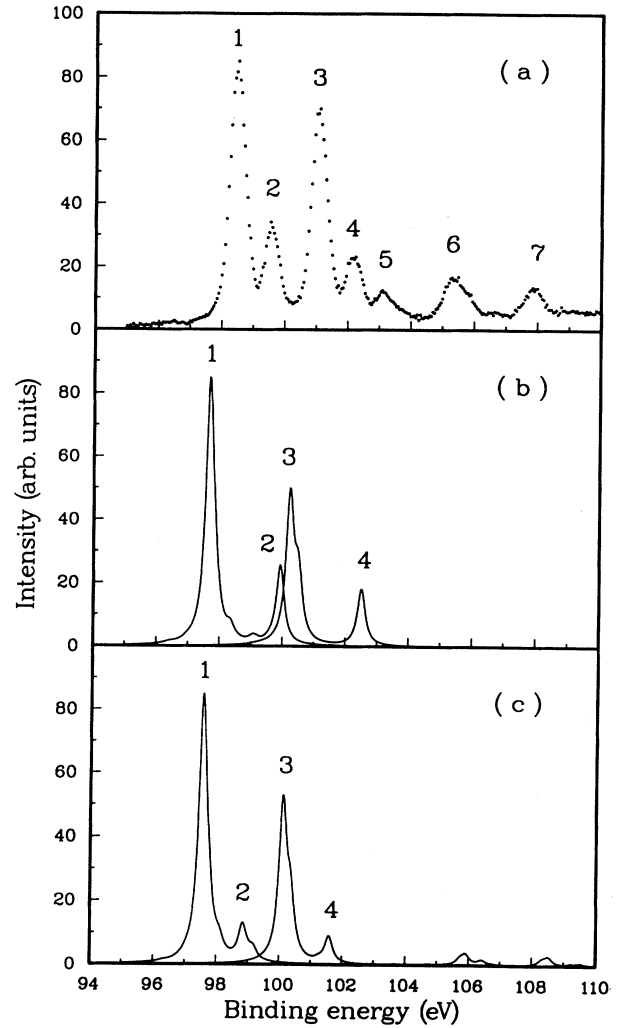


FIG. 4. The Ba $4d_{5/2,3/2}$ photoelectron spectrum: (a) experiment, (b) truncated-set calculation, and (c) calculation, based on set (11). Peak 1 has been normalized to the same height in all spectra. The peaks 1 and 2 are associated with the $4d_{5/2}$ hole, and the peaks 3 and 4 with the $4d_{3/2}$ hole.

the total decay rate of a state $\Psi_\beta(J_\beta M_\beta)$ [10]. The quantities $T_{f\beta}$ involve the Auger amplitudes and the Auger partial wave phase shifts. The anisotropy is a consequence of alignment; the electron-impact cross sections $Q_\beta(J_\beta M_\beta)$ depend in principle on the magnetic quantum numbers M_β provided $J_\beta > 1/2$. This is true for creation of 4d hole states (1) of Ba^+ . The angle-averaged number of emitted Auger electrons, which is obtained from Eq. (2) by integrating over θ , is proportional to the product of the total cross section $Q_\beta(J_\beta) = \sum_{M_\beta} Q_\beta(J_\beta M_\beta)$ and the Auger component rate

$$T_{f\beta}(J_f, J_\beta) = \frac{2\pi}{\hbar} \sum_{l_A, j_A} \left| \sum_\nu \sum_\mu c_{\beta\nu} c_{f\mu} \left\langle \Phi_\mu(J_f) \varepsilon_{Al} j_A; J_\beta M_\beta \left| \sum_{\lambda, \lambda'=1}^{N_e-1} V_{\lambda\lambda'} \right| \Phi_\nu(J_\beta M_\beta) \right\rangle \right|^2, \quad (3)$$

where the final-ionic-state CSF's $\Phi_\mu(J_f M_f)$ has been coupled to the energy normalized continuum orbitals $|\varepsilon_A l_A j_A m_A\rangle$ of the Auger electron to yield antisymmetrized final-state wave functions $|J_\beta M_\beta\rangle$ which have the same parity as the CSF's $\Phi_\nu(J_\beta M_\beta)$ in Eq. (1). The two-electron operator $V_{\lambda\lambda'}$ is taken to be the sum of the Coulomb and transverse Breit operators [11].

We shall, following Rose, Grant, and Connerade [12], approximate the total cross section $Q_\beta(J_\beta)$ by the relative Bethe-Born cross section

$$Q_\beta(J_\beta) = \frac{1}{(2J_i + 1)} \sum_{J_\gamma, l_j} \sum_{M_i} \sum_{M_\gamma} \int \left| \sum_\nu \sum_\alpha c_{\beta\nu} c_{i\alpha} \left\langle \Phi_\nu(J_\beta) \varepsilon l j; J_\gamma M_\gamma \left| \sum_{\lambda=1}^{N_e} x_\lambda \right| \Phi_\alpha(J_i M_i) \right\rangle \right|^2 d\varepsilon$$

$$= \frac{1}{3} \sum_{J_\gamma, l_j} \int \left| \sum_\nu \sum_\alpha c_{\beta\nu} c_{i\alpha} \left\langle \Phi_\alpha(J_i) \left\| \sum_{\lambda=1}^{N_e} r_\lambda \mathbf{C}_1(\theta_\lambda) \right\| \Phi_\nu(J_\beta) \varepsilon l j; J_\gamma \right\rangle \right|^2 d\varepsilon, \quad (4)$$

where it is assumed that the initial ionic CSF's $\Phi_\nu(J_\beta M_\beta)$ have been coupled to the energy normalized continuum orbitals $|\varepsilon l j m\rangle$ of the ejected electron to yield antisymmetrized intermediate-state wave functions $|J_\gamma M_\gamma\rangle$, subject to the dipole selection rules. In Eq. (4) the axis of quantization coincides with the direction of the momentum transfer \mathbf{K} in $x_\lambda = \mathbf{K} \cdot \mathbf{r}_\lambda$ rather than with the beam axis as in Eq. (2). This choice is possible since there is a summation over M_i and M_γ in Eq. (4) which results in the factor 1/3 in front of the reduced matrix element [13], after switching the position of $\Phi_\alpha(J_i M_i)$ and $|J_\beta M_\beta\rangle$. The use of the dipole approximation implies that the angular distribution is of the form $1 + A_2 P_2(\cos \theta)$, where A_2 is the anisotropy coefficient [10]. If the detector is set at the magic angle $\theta_m = 54.7^\circ$ with respect to the beam axis for which $P_2(\cos \theta_m) = 0$, the angle-averaged number of Auger electrons, proportional to the product $Q_\beta(J_\beta) T_{f\beta}(J_f, J_\beta)$, is recorded. According to Sec. II this condition is fulfilled in our experiment.

Since a set of orthonormal self-consistent central-field Dirac-Fock orbitals are used to construct the CSF's, the many-electron reduced matrix elements in Eq. (4) can be simplified by a decomposition of the appropriate wave functions into an antisymmetric product of $N_e - 1$ electron wave functions and the orbital of the active electron [13]. The general result has been described by Pyper, Grant, and Beatham [14] in connection with their description of a program which calculates matrix elements of one-particle operators in jj coupling.

As an application we consider ionization from an inner-filled subshell $(n_\alpha j_\alpha)^{2j_\alpha+1}$ of a closed-shell atom such as Ba ($J_i = 0$). The mixing of the CSF's is assumed to be a consequence of assigning several configurations to the outer shells. The evaluation [12] of the reduced matrix elements in Eq. (4) yields

$$Q_\beta(J_\beta) = \frac{1}{3} Q'_\beta(J_\beta) \sum_{i,j} \int |\langle n_\alpha l_\alpha j_\alpha || r \mathbf{C}_1 || \varepsilon l j \rangle|^2 d\varepsilon, \quad (5)$$

where

$$Q'_\beta(J_\beta) = (2j_\alpha + 1) \left| \sum_\nu \sum_\alpha c_{\beta\nu} c_{i\alpha} \delta_{X_\nu Y_\alpha} \right|^2 \quad (6)$$

is the relative partial photoionization cross section, integrated over all directions of the photoelectron. Here X_ν refers to the configuration which is associated with $\Phi_\nu(J_\beta M_\beta)$ and Y_α to the same parent configuration after coupling an $n_\alpha j_\alpha$ orbital from $\Phi_\alpha(J_i M_i)$.

The factorization of $Q_\beta(J_\beta)$ into $Q'_\beta(J_\beta)$ and an effective single-electron cross section in Eq. (5) is based on two approximations.

(i) The same set of orthogonal orbitals has been used to construct both the initial CSF's $\Phi_\alpha(J_i M_i)$ and the intermediate ionic CSF's $\Phi_\nu(J_\beta M_\beta)$ in Eq. (4). This approximation excludes the effect of relaxation upon the cross sections (4).

(ii) The continuum orbitals $|\varepsilon l j m\rangle$ have been evaluated in an average jj potential of the initial ionic-state configurations by keeping the bound orbitals fixed. This procedure yields continuum orbitals which are independent of β and ν in accordance with Eq. (5).

If it is assumed that the total decay probability $P_\beta(J_\beta)$ in Eq. (2) is independent of β and J_β we have in accordance with Eqs. (2), (3), and (5) that

$$n'_{f\beta}(J_f J_\beta) = T_{f\beta}(J_f, J_\beta) Q'_\beta(J_\beta), \quad (7)$$

which relates the relative number of Auger electrons emitted in high-energy electron impact to the relative partial photoionization cross section (6).

The cross-section formula (6) is consistent with the generalized sudden approximation theory of photoionization [15] and with the explicit formulation of Martin and Shirley [16], who considered the appearance of correlation satellites in photoelectron spectra as a consequence of both initial- and final-state CI. Equation (6) can be used to construct a photoelectron spectrum on a relative intensity scale once the binding energies

$$I_\beta^+ = E_\beta(J_\beta) - E_i(J_i) = \hbar\omega - E'_{\text{kin}} \quad (8)$$

or the kinetic energies E'_{kin} are known. The related Auger spectrum may be obtained using Eq. (7) and the kinetic Auger electron energies

$$E_{\text{kin}} = E_\beta(J_\beta) - E_f(J_f) = I_\beta^+ - I_f^{++}, \quad (9)$$

where $I_f^{++} = E_f(J_f) - E_i(J_i)$. The energies (8) and (9) are usually calculated using the ΔE_{SCF} method which involves separate optimization of initial-, intermediate-, and final-state orbitals by self-consistent-field procedures for a given transition. In both the photoelectron and Auger electron case the lifetime broadening can be taken into account by multiplying the expressions (6) and (7) by a normalized Lorentzian of width $\Gamma_\beta = \hbar P_\beta(J_\beta)$ and $\Gamma_A = \Gamma_\beta + \Gamma_f$, respectively. If the coefficients $c_{f\mu}$ in

Eq. (3) represent the ground state of the residual doubly charged ion $\Gamma_f = 0$.

IV. RESULTS AND DISCUSSION

A. Calculations

In principle we should deal with ISCI, IMISCI, and FISCI in the sequence

$$\begin{aligned}
 4d^{10}5s^25p^66s^2(J_i = 0) &\rightarrow \left\{ \begin{array}{l} \text{photoionization} \\ \text{electron impact} \end{array} \right\} \\
 &\rightarrow 4d^95s^25p^66s^2(J_\beta = 3/2, 5/2) \rightarrow \text{Auger decay} \\
 &\rightarrow 4d^{10}5s^25p^6(J_f = 0),
 \end{aligned} \tag{10}$$

where the principal configurations outside the Kr core of Ba are given without explicit indication of spin-orbit splitting. It is reasonable, however, to neglect both ISCI and FISCI. For the Ba ground state the lowest-energy ASF is dominated by the $6s^2$ CSF in accordance with Eq. (10). Two very different types of CI calculations [12, 17] indicate that $c_{i1}^2 \cong 0.90$ independently of the number of configurations other than $6s^2$. A considerable redistribution of weights may occur among the additional CSF's as their number is increasing, but that should not affect c_{i1} very much. Consequently, we have used a single $6s^2$ CSF to represent the ground state of Ba. Since $6s^2$ is missing from the final-state configuration in the sequence (10) we have used a single CSF for that configuration as well.

With single initial- and final-ionic CSF's in the two-step process (10) any satellite structure or deviation from the statistical $4d_{5/2}:4d_{3/2}$ ratio can only be attributed to 4d hole IMISCI if relaxation is neglected. We have considered two sets of configurations. The extended set is represented by

$$4d^9(6s^2 + 5d6s + 5d^2 + 4f^2 + 6p^2) \tag{11}$$

whereas the truncated set does not include $4f^2$ and $6p^2$. Calculations were also made with intermediate sets which included either $4f^2$ or $6p^2$ but it did not change the truncated-set results significantly. The CI equation (11) including the 4d spin-orbit splitting results in 46 CSF's for $J_\beta = 3/2$ and 52 CSF's for $J_\beta = 5/2$ provided the $4d_{3/2}$ orbital is also included in the $J_\beta = 5/2$ set and vice versa. The corresponding numbers for the truncated set are 23 and 25, respectively.

The MCDF-AL procedure [18] was used to generate the 98 ASF's corresponding to the set (11) in separate calculations for $J_\beta = 3/2$ and $5/2$, respectively. The resulting DF orbitals were also used in the intermediate- and final-ionic CSF's. The same procedure was used for the truncated set. The energies of the initial, intermediate-ionic, and final-ionic ASF's were calculated using the ΔE_{SCF} method including the Breit interaction. The Auger component rates (3) were calculated using the

single-channel version of our multichannel multiconfiguration Dirac-Fock program [19].

Since only the principal initial-state $6s^2$ CSF has been taken into account, it follows from Eq. (6) that

$$Q'_\beta(J_\beta) = (2J_\beta + 1)c_{\beta i}^2, \tag{12}$$

where the coefficient $c_{\beta i}$ represents the corresponding uniquely defined parent configuration in the ASF expansion (1). In contrast, all coefficients $c_{\beta\nu}$ appear in the transition rates (3), where $c_{f\mu} = \delta_{f\mu}$.

Equation (12) was used together with ΔE_{SCF} calculations of binding energies (8) to generate a photoelectron spectrum as a function of the binding energy. Each line was represented by a Lorentzian function of width $\Gamma_\beta = 0.3$ eV [20]. The Auger electron spectrum can be considered in accordance with Eqs. (7)–(9) to be the photoelectron spectrum weighted by the transition rates (3) and shifted towards lower energies by $\Delta = E_f(0) - E_i(0) = 13.64$ eV, which is the ΔE_{SCF} ionization energy of removing both 6s electrons.

The results which correspond to the use of set (11) are given in Table I for $J_\beta = 3/2$ and $5/2$, respectively. Each Auger electron or binding energy corresponds to an ASF numbered from 1 to 46 ($J_\beta = 3/2$) and 52 ($J_\beta = 5/2$) in the first column. The second column gives the principal nonrelativistic configuration contribution in the form wx , where w is the weight and $x = 6s^2, 5d6s, 5d^2, 4f^2$, or $6p^2$. The weight w has been obtained by transforming the ASF's from the jj basis to an LS basis from which the weight had been obtained by summing over the appropriate coefficients after squaring [21]. The third column lists the Auger electron energy (9), which is related to the binding energy (8) by the shift $-\Delta$. The fourth column gives the relative partial photoionization cross section (12), the fifth column the Auger rate (3) in the units of 10^{-3} a.u., and the sixth column the relative number (7) of emitted Auger electrons in high-energy electron impact or photoionization. We shall analyze on the basis of Table I the photoelectron and Auger electron spectrum separately in the following. The most salient results of our analysis are summarized in Fig. 5.

B. Photoelectron spectrum

Figure 4 shows the experimental $4d$ photoelectron spectrum in comparison with the calculated spectra which cover a larger energy range according to Table I. Figure 4(b) was obtained without the $4f^2$ and $6p^2$ configurations in Eq. (11). The inclusion of either one of these configurations did not change the spectrum very

much while the inclusion of both resulted in the spectrum shown in Fig. 4(c). According to Table I the peaks 1 and 2 are associated with the $4d_{5/2}$ hole whereas 3 and 4 belong to the $4d_{3/2}$ hole. Both doublets, which are separated by spin-orbit splitting 2.6 eV, are related to several ASF's. Peak 1 can thus be attributed to ASF's 11–13 ($J_\beta = 5/2$), peak 2 to 14 and 17 ($J_\beta = 5/2$), peak 3 to 19 and 21 ($J_\beta = 3/2$), and peak 4 to 22 and 23

TABLE I. Theoretical Auger electron energy E_{kin} , relative photoionization and electron impact cross section [Eq. (12)], Auger decay rate [Eq. (3)], and relative number of emitted Auger electrons for each atomic state function [Eq. (7)].

ASF number	$4d_{3/2}$					$4d_{5/2}$				
	Character ^a	E_{kin}^b	Eq. (12)	Eq. (3) ^c	Eq. (7)	Character ^a	E_{kin}^b	Eq. (12)	Eq. (3) ^c	Eq. (7)
1	0.98 $5d^2$	82.41	0.00000	0.00045	0.00000	0.98 $5d^2$	82.40	0.00162	0.00041	0.00000
2	0.98 $5d6s$	82.54	0.00000	0.00003	0.00000	0.89 $5d^2$	82.64	0.01176	0.00007	0.00000
3	0.95 $5d^2$	82.71	0.00004	0.00078	0.00000	0.97 $5d^2$	82.77	0.00192	0.00001	0.00000
4	0.84 $5d^2$	82.77	0.00004	0.00000	0.00000	0.97 $5d6s$	83.09	0.00198	0.00006	0.00000
5	0.51 $5d^2$	83.08	0.00004	0.00194	0.00000	0.97 $5d^2$	83.28	0.00318	0.00019	0.00000
6	0.77 $5d6s$	83.10	0.00004	0.00109	0.00000	0.53 $5d6s$	83.35	0.00864	0.01413	0.00012
7	0.94 $5d^2$	83.32	0.00004	0.00000	0.00000	0.65 $5d6s$	83.42	0.02298	0.01556	0.00036
8	0.93 $5d6s$	83.45	0.00108	0.00051	0.00000	0.99 $5d6s$	83.49	0.01044	0.00052	0.00000
9	0.94 $5d^2$	83.80	0.00000	0.00922	0.00000	0.97 $5d^2$	83.67	0.03054	0.00064	0.00002
10	0.85 $5d^2$	84.16	0.00096	0.14505	0.00014	0.97 $5d^2$	83.71	0.00018	0.00005	0.00000
11	0.57 $5d^2$	84.38	0.00024	0.07031	0.00002	0.66 $6s^2$	83.91	3.98484	0.00192	0.00765
12	0.99 $5d^2$	85.13	0.00008	0.00120	0.00000	0.81 $5d^2$	84.09	0.54954	0.10003	0.05497
13	0.53 $5d6s$	85.39	0.00340	0.00042	0.00000	0.53 $5d6s$	84.46	0.20214	0.04561	0.00922
14	0.67 $5d6s$	85.45	0.00452	0.00101	0.00000	0.79 $5d^2$	85.17	0.46974	0.00473	0.00222
15	0.97 $5d6s$	85.78	0.01204	0.00041	0.00000	0.98 $5d^2$	85.23	0.07098	0.00000	0.00000
16	0.93 $5d^2$	85.83	0.00024	0.00118	0.00000	0.97 $5d^2$	85.34	0.04218	0.00100	0.00004
17	0.98 $5d6s$	86.01	0.00800	0.00063	0.00000	0.82 $5d^2$	85.51	0.17094	0.01087	0.00186
18	0.96 $5d^2$	86.19	0.00040	0.00611	0.00000	0.96 $5d6s$	85.60	0.00216	0.00048	0.00000
19	0.58 $6s^2$	86.44	2.40520	0.00751	0.01806	0.88 $5d^2$	85.87	0.00408	0.00131	0.00000
20	0.97 $5d^2$	86.46	0.00088	0.00199	0.00000	0.57 $5d6s$	85.93	0.00234	0.00787	0.00002
21	0.42 $5d6s$	86.70	0.84404	0.19592	0.16536	0.52 $5d^2$	85.95	0.00090	0.01724	0.00002
22	0.84 $5d^2$	87.59	0.03620	0.93205	0.03374	0.97 $5d6s$	86.09	0.00054	0.00044	0.00000
23	0.80 $5d^2$	87.93	0.41096	0.31630	0.12999	0.98 $5d^2$	86.25	0.00000	0.00003	0.00000
24	0.98 $6p^2$	90.07	0.00004	0.00082	0.00000	0.71 $5d6s$	87.08	0.00018	0.01118	0.00000
25	0.99 $6p^2$	90.35	0.00000	0.00032	0.00000	0.97 $5d^2$	88.00	0.00024	1.37726	0.00033
26	0.98 $4f^2$	90.79	0.00000	0.00013	0.00000	0.96 $6p^2$	90.00	0.01074	0.00019	0.00000
27	0.94 $6p^2$	90.98	0.00040	0.00018	0.00000	0.99 $6p^2$	90.20	0.00054	0.00001	0.00000
28	0.97 $4f^2$	91.96	0.00008	0.00001	0.00000	0.98 $6p^2$	90.34	0.00000	0.00009	0.00000
29	0.96 $4f^2$	92.40	0.00000	0.00289	0.00000	0.97 $4f^2$	90.69	0.00000	0.00000	0.00000
30	0.95 $6p^2$	92.59	0.00592	0.00001	0.00000	0.77 $6p^2$	91.06	0.01068	0.00183	0.00002
31	0.96 $6p^2$	92.68	0.00004	0.00014	0.00000	0.78 $4f^2$	91.59	0.00216	0.00079	0.00000
32	0.98 $6p^2$	92.92	0.00028	0.00001	0.00000	0.97 $4f^2$	91.68	0.00060	0.00056	0.00000
33	0.97 $4f^2$	93.11	0.00004	0.00169	0.00000	0.73 $4f^2$	92.07	0.08034	0.00046	0.00004
34	0.95 $4f^2$	93.15	0.00028	0.00011	0.00000	0.57 $4f^2$	92.25	0.14460	0.00002	0.00000
35	0.67 $4f^2$	93.59	0.00156	0.00002	0.00000	0.81 $4f^2$	92.75	0.06726	0.00007	0.00000
36	0.62 $6p^2$	93.70	0.00012	0.00021	0.00000	0.97 $6p^2$	92.77	0.00192	0.00000	0.00000
37	0.98 $4f^2$	94.31	0.00032	0.00901	0.00000	0.92 $6p^2$	92.86	0.00132	0.00001	0.00000
38	0.78 $4f^2$	94.65	0.06884	0.00355	0.00024	0.91 $4f^2$	93.08	0.00996	0.00005	0.00000
39	0.55 $6p^2$	94.86	0.11584	0.00201	0.00023	0.95 $4f^2$	93.40	0.00222	0.00051	0.00000
40	0.98 $4f^2$	95.11	0.00024	0.00000	0.00000	0.88 $4f^2$	93.74	0.00012	0.00029	0.00000
41	0.88 $4f^2$	95.59	0.02640	0.00031	0.00001	0.74 $6p^2$	93.78	0.00714	0.00137	0.00001
42	0.96 $4f^2$	96.20	0.00444	0.00050	0.00000	0.97 $4f^2$	94.06	0.00000	0.00019	0.00000
43	0.98 $4f^2$	96.70	0.00120	0.00122	0.00000	0.93 $4f^2$	94.31	0.00090	0.00118	0.00000
44	0.98 $4f^2$	97.49	0.00096	0.00018	0.00000	0.93 $4f^2$	94.58	0.00120	0.00293	0.00000
45	0.86 $4f^2$	98.45	0.04048	0.00415	0.00017	0.98 $4f^2$	95.08	0.00030	0.00174	0.00000
46	0.99 $4f^2$	104.06	0.00048	0.51616	0.00024	0.97 $4f^2$	95.13	0.00624	0.00002	0.00000
47						0.93 $4f^2$	95.70	0.01806	0.00093	0.00002
48						0.93 $4f^2$	95.88	0.02706	0.00167	0.00005
49						0.96 $4f^2$	96.40	0.01104	0.00255	0.00003
50						0.98 $4f^2$	96.87	0.00132	0.00124	0.00000
51						0.99 $4f^2$	104.21	0.00024	0.37251	0.00008
52						0.99 $4f^2$	104.79	0.00000	0.00186	0.00000

^a Character is given by the principal nonrelativistic configuration and its weight.

^b The Auger electron energy E_{kin} is related to the binding energy I_β^+ [Eq. (8)] by $E_{\text{kin}} = I_\beta^+ - \Delta$, where $\Delta = 13.64$ eV according to ΔE_{SCF} calculations.

^c The Auger rates are given in units of 10^{-3} a.u.

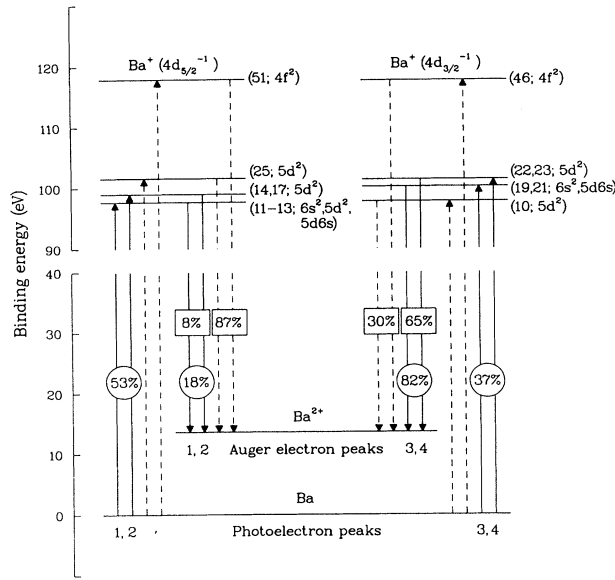


FIG. 5. Schematic configuration-interaction model [Eq. (11)] diagram of the creation of Ba 4d hole states and their subsequent Auger decay into the Ba^{2+} ground state. The solid arrows represent the pathways which give rise to the peaks 1–4 in Fig. 3 (Auger electron spectrum) and Fig. 4 (photoelectron spectrum). The circled figures represent the calculated relative numbers of emitted electrons in both processes. The dashed arrows represent “forbidden” pathways which do not populate 4d hole states but which have a very high Auger rate. The calculated relative Auger rates in the boxes illustrate the dramatic difference between the decay pattern of the $4d_{3/2}$ and $4d_{5/2}$ hole states. The numbers in the parentheses refer to the corresponding atomic-state functions in Table I, followed by the corresponding principal nonrelativistic configurations.

($J_\beta = 3/2$). Nevertheless, peaks 1 and 3 have predominantly $6s^2$ character according to Table I, which classifies 2 and 4 as CI satellites with predominantly $5d^2$ character. Since $\sum Q'_\beta(J_\beta) = 2J_\beta + 1$ according to Eq. (12) the ratio of all $J_\beta = 5/2$ lines to all $J_\beta = 3/2$ lines is statistical. What has been measured, however, is the ratio of peak 1 to 3, which is 1.2 ± 0.2 according to Sec. II. From Fig. 5 the ratio of (peak 1 plus peak 2) to (peak 3 plus peak 4) is 1.43 in reasonable agreement with experiment.

The energy region from 102 to 109 eV, which incorporates three prominent peaks labeled 5–7 in Fig. 4(a), is poorly represented by our calculations, although some CI satellite structure appears in this region according to Fig. 4(c). One reason for this discrepancy is the neglect of relaxation which gives rise to $6s \rightarrow ns$ shakeup satellites in the region of peaks 5 and 6 [9]. A simple calculation of overlap integral indicates that the $4d_{3/2}$ and $4d_{5/2}$ $6s \rightarrow 7s$ shakeup satellites have each an intensity which is about 8% of the intensity of the corresponding main peak. A full analysis which should be based on separately optimized ASF's for the initial and 4d hole states would probably reveal combined effects of CI and relaxation.

The main result of our analysis of the 4d photoelectron spectrum is the interpretation of the strongest peaks 1–

TABLE II. Experimental and calculated energies of the peaks 1–4 in the Ba $4d^{-1} \rightarrow 6s^{-2}$ Auger spectrum (Fig. 3) and in the Ba 4d photoelectron spectrum (Fig. 4).

Peak	Auger electron spectrum		Photoelectron spectrum	
	Expt.	Calc. ^a	Expt.	Calc. ^b
1	83.1 ± 0.2	84.12	98.3 ± 0.2	97.59
2	84.2 ± 0.2	85.33	99.4 ± 0.2	98.90
3	85.7 ± 0.2	86.67	100.9 ± 0.2	100.15
4	86.8 ± 0.2	87.86	102.0 ± 0.2	101.54

^a The Auger electron energies have been calculated as weighted averages with weights given in the sixth and eleventh columns [Eq. (7)] of Table I.

^b The binding energies have been calculated as weighted averages with weights given in the fourth and ninth columns [Eq. (12)] of Table I.

4. A comparison of Figs. 4(a) and 4(c) shows that not only the $4d_{5/2}:4d_{3/2}$ branching ratio comes about right, but also that the intensity of satellites relative to those of corresponding main peaks is predicted rather well by our MCDF model. According to Table II the ΔE_{SCF} calculations yield binding energies including the spin-orbit splitting which are in good agreement with experiment.

C. Auger electron spectrum

Figure 3 shows the experimental $4d^{-1} \rightarrow 6s^{-2}$ Auger electron spectrum in comparison with part of the calculated spectra. Figure 3(b) was obtained without the $4f^2$ and $6p^2$ configurations in set (11). The results of the complete CI calculation, which is shown in Fig. 3(c), are listed in Table I. The sum of the $J_\beta = 3/2$ Auger rates is 2.238×10^{-3} a.u. whereas it is 2.005×10^{-3} a.u. for $J_\beta = 5/2$. The difference, which is not very large, is due to slightly different Slater integrals in the $4d_{3/2}$ and $4d_{5/2}$ Auger amplitudes. In contrast, the summation of the relative yields of emitted Auger electrons, listed in the sixth column, gives $n'(J_\beta = 5/2):n'(J_\beta = 3/2) = 0.22$. This ratio is much smaller than statistical ratio 1.5, which approximately relates the number of $4d_{5/2}$ electrons to the number of $4d_{3/2}$ electrons, produced in primary ionization. Consequently, the distribution of the Auger rates among the initial 4d hole ASF's is very different depending on whether $J_\beta = 5/2$ or $3/2$. According to our model it leads to a sevenfold reduction of the production of $J_\beta = 5/2$ Auger electrons relative to the production of $J_\beta = 3/2$ Auger electrons. Would there be no CI in the intermediate 4d hole states the ratio would be 1.5 and there would be no quenching.

According to Table I the ASF's 11–13 contribute to peak 1, and the ASF's 14 and 17 to peak 2 in the $J_\beta = 5/2$ part of the Auger spectrum. These ASF's are also responsible for peaks 1 and 2 in the photoelectron spectrum. The intensity ratio of peak 1 to 2 is somewhat different due to the weighting by the Auger rates in accordance with Eq. (7). A comparison of the $J_\beta = 3/2$ part of the spectra in Figs. 3(c) and 4(c) indicates a large difference in the intensity ratio of peak 3 to 4. Also in this case the same ASF's are responsible for the doublet structure; peak 3 is due to ASF's 19 and 21, and peak 4 to 22 and 23 in both spectra. The difference in the ratio is thus

a consequence of large variations in the Auger rates. A comparison of Figs. 4(c) and 3(c) also demonstrates the predicted reversal of the intensity ratio of $J_\beta = 5/2$ to $J_\beta = 3/2$ in going from the photoelectron to the Auger electron spectrum.

Table II shows that the ΔE_{SCF} calculations for the extended set (11) predict the positions of the Auger lines rather well. The identification of 1 and 3 as $6s^2$ main lines and 2 and 4 as $5d^2$ satellite lines is less clear for the Auger electron than for the photoelectron spectrum. The weighting by the Auger rates tends to reduce the significance of the $6s^2$ contribution. For example, peak 1 mainly originates from ASF 12 with predominantly $5d^2$ character whereas the corresponding peak in the photoelectron spectrum is dominated by ASF 11 with the largest $6s^2$ weight according to Table I. The discrepancy between the calculated and experimental spectra is mainly due to a poor prediction of the intensity ratio of satellites 2 and 4. Removal of intensity from 4 to 2 would bring the calculated intensity ratio of the $4d_{5/2}$ to $4d_{3/2}$ peaks [(peak 1 plus peak 2):(peak 3 plus peak 4)] closer to the measured value 0.8 ± 0.2 . A comparison of the spectra in Figs. 3(b) and 3(c) shows how sensitive the positions and relative intensities of 2 and 4 are to the choice of the basis set. The omission of the dependence of the total decay rate $P_\beta(J_\beta)$ [Eq. (2)] on β and J_β seems not to explain the discrepancy between the extended-set calculation and experiment since $P_\beta(J_\beta)$ is governed by $N_{4,5}OO$ inner-shell transitions.

The radial Slater integrals which appear in the Auger amplitudes are all of the form $R^k(4d\epsilon dnl'n'l')$, where $nln'l'$ refers to the two-electron configurations in Eq. (11). The $5d^2$ and $4f^2$ configurations give rise, as a consequence of partial collapse, to some $|R^k|$ values which are larger than $|R^2(4d\epsilon d6s6s)| \simeq 0.003$ a.u. by as much as a factor of 3. Whether the orbitals have $j = l - 1/2$ or $j = l + 1/2$ is of less importance. The variation among the absolute values of the possible R^k 's is not very large however; we find that 0.001 a.u. $\leq |R^k| \leq 0.01$ a.u., regardless the value of $k \leq 5$ and the orbitals involved. This behavior leads to significant Auger amplitudes for all configurations in set (11) and for $5d^2$ and $4f^2$, in particular. The anomalously small $4d_{5/2}:4d_{3/2}$ branching ratio is thus not only a consequence of the behavior of the R^k 's but also a consequence of a mismatch between primary ionization and Auger decay for $J_\beta = 5/2$. The $6s^2$ character of the ASF's 11–14 and 17 explains the most salient features of the $J_\beta = 5/2$ part of the photoelectron spectrum. According to Table I and Fig. 5 these states participate only by 8%, however, in Auger decay to the final $4d^{10}5s^25p^6$, $J_f = 0$ state. As Table I shows, the ASF 25 with very strong $5d^2$ character is responsible for 69% and the ASF 51 with very strong $4f^2$ character for 19% of all $J_\beta = 5/2$

Auger $4d^{-1} \rightarrow 6s^{-2}$ transitions. Since these states have a very small $6s^2$ contribution their production probability is negligible in primary ionization, and hence there is a quenching of the $J_\beta = 5/2$ Auger decay.

In the case of $J_\beta = 3/2$ this mismatch occurs to a lesser extent. The ASF's 19 and 20–23, which are responsible for the corresponding photoelectron distribution, decay according to Table I and Fig. 5 with a relative probability of 65% to the Ba^{2+} ground state. The ASF 22 with strong $5d^2$ character is responsible for both the satellite structure in the photoelectron spectrum and most of the Auger decay. As Table I shows, there is a loss of 23% of the Auger decay through ASF 46 which with its strong $4f^2$ character is not appreciably populated in primary ionization. It also follows from Table I that the photoelectron structures, labeled 5–7 in Fig. 3(a), should not have a counterpart in the Auger spectrum to the extent they are due to CI of type (11).

Our findings regarding the $\text{Ba } 4d^{-1} \rightarrow 6s^{-2}$ spectrum should be compared with a similar but less successful interpretation of the $\text{Ca } 2p^{-1} \rightarrow 4s^{-2}$ spectrum [4]. In the Ca case the set $2p^5(4s^2 + 3d4s + 3d^2 + 4s5s + 4p^2)$ with $J_\beta = 1/2$ and $3/2$ leads to a pattern which completely disagrees with the experiment. The measurement indicates that the $2p_{3/2}:2p_{1/2}$ branching ratio is about 2 whereas a calculation based on a truncated set without $4s5s$ and $4p^2$ predicted a ratio close to one. This once again uncovers the danger to draw too far-reaching conclusions from limited-basis-set MCDF calculations without combining evidence from both photoelectron and Auger electron spectra as we have done.

V. CONCLUSIONS

It has been demonstrated that intermediate-ionic-state configuration interaction of the $\text{Ba}^+ 4d$ hole leads to an interpretation of the doublet structure in both the $4d_{5/2,3/2}$ photoelectron and $4d_{5/2,3/2}^{-1} \rightarrow 6s^{-2}$ Auger electron spectrum. Our results show that the nonstatistical $4d_{5/2}:4d_{3/2}$ branching ratio in the Auger spectrum is independent of the mode of excitation in accordance with experiments. The anomalously low value of this ratio is attributed in accordance with Fig. 5 to $4d_{5/2}$ hole states which have a large Auger decay probability but which are not populated in the primary ionization process. Our analysis clearly demonstrates that a correct treatment of the radiationless decay of strongly correlated hole states is impossible without including the distribution of the primary-ionization probabilities.

ACKNOWLEDGMENTS

The authors thank J. E. Hansen for helpful discussions. This work has been supported by the Research Council for the Natural Sciences of the Academy of Finland.

- [1] M. Richter, M. Meyer, M. Pahler, T. Prescher, E. v. Raven, B. Sonntag, and H. E. Wetzels, Phys. Rev. A **39**, 5666 (1989).
- [2] J. M. Bizau, D. Cubaynes, P. Gérard, and F. J. Wuilleumier, Phys. Rev. A **40**, 3002 (1989).
- [3] J. P. Connerade and M. A. Baig, in *Handbook on Syn-*

chrotron Radiation, edited by G. V. Marr (Elsevier, Amsterdam, 1987), Vol. 2, p. 175, and references therein.

- [4] W. Weber, B. Breuckmann, R. Huster, W. Menzel, W. Mehlhorn, M. H. Chen, and K. G. Dylla, J. Electron. Spectrosc. Relat. Phenom. **47**, 105 (1988); M. H. Chen, W. Weber, and W. Mehlhorn, *ibid.* **49**, 77 (1989).

- [5] W. Mehlhorn, B. Breuckmann, and D. Hausmann, *Phys. Scr.* **16**, 177 (1977).
- [6] M. Kellokumpu and H. Aksela, *Phys. Rev. A* **31**, 777 (1985).
- [7] Unpublished results by U. Becker, H. G. Kerkhoff, M. Kupsch, B. Langer, A. Sivasli, and R. Wehlitz (unpublished), quoted in Ref. [8].
- [8] V. Radojević, M. Kutzner, and H. P. Kelly, *Phys. Rev. A* **40**, 727 (1989).
- [9] A. Mäntykenttä, H. Aksela, S. Aksela, A. Yagishita, and E. Shigemasa, *J. Phys. B* **25**, 5315 (1992).
- [10] T. Åberg and G. Howat, in *Encyclopedia of Physics*, edited by S. Flügge and W. Mehlhorn (Springer, Berlin, 1982), Vol. 31, p. 469.
- [11] H. Aksela, S. Aksela, J. Tulkki, T. Åberg, G. M. Bancroft, and K. H. Tan, *Phys. Rev. A* **39**, 3401 (1989).
- [12] S. J. Rose, I. P. Grant, and J. P. Connerade, *Philos. Trans. R. Soc. London Ser. A* **269**, 527 (1980).
- [13] D. M. Brink and G. R. Satchler, *Angular Momentum*, 2nd ed. (Clarendon, Oxford, 1968).
- [14] N. C. Pyper, I. P. Grant, and N. A. Beatham, *Comput. Phys. Commun.* **15**, 387 (1978).
- [15] T. Åberg, *Ann. Acad. Sci. Fenn. Ser. A6* **308**, 1 (1969).
- [16] R. L. Martin and D. A. Shirley, *J. Chem. Phys.* **64**, 3685 (1976); *Phys. Rev. A* **13**, 1475 (1976).
- [17] H. Bergeron and A. Valance, *Z. Phys. D* **6**, 309 (1987).
- [18] I. P. Grant, B. J. McKenzie, P. H. Norrington, M. F. Mayers, and N. C. Pyper, *Comput. Phys. Commun.* **21**, 207 (1980).
- [19] J. Tulkki, T. Åberg, A. Mäntykenttä, and H. Aksela, *Phys. Rev. A* **46**, 1357 (1992).
- [20] $\Gamma_\beta = 0.30 \pm 0.05$ eV was determined from the spectrum shown in Fig. 4(a).
- [21] K. G. Dyall, I. P. Grant, C. T. Johnson, F. A. Parpia, and E. P. Plummer, *Comput. Phys. Commun.* **55**, 425 (1989).